Geothermics 83 (2020) 101721

Contents lists available at ScienceDirect

Geothermics

journal homepage: www.elsevier.com/locate/geothermics

# Impact of groundwater heat pump systems on subsurface temperature under variable advection, conduction and dispersion

William Pophillat[a], Peter Bayer[b], Esther Teyssier[c], Philipp Blum[d], Guillaume Attard[a,*]

[a] Cerema, Département Environnement Territoires Climat, 46 rue Saint-Théobald, F-38081, L'Isle d'Abeau, France
[b] Ingolstadt University of Applied Sciences, Institute of new Energy Systems (InES), Esplanade 10, 85049, Ingolstadt, Germany
[c] Nepsen, Sintec ingénierie, 2-4 Allée de Lodz, 69007, Lyon, France
[d] Karlsruhe Institute of Technology (KIT), Institute of Applied Geosciences (AGW), Kaiserstraße 12, 76131, Karlsruhe, Germany

ARTICLE INFO

*Keywords:*
Thermal impact
Shallow geothermal energy
Groundwater heat pump
Open-loop
Numerical modelling
Aquifer

ABSTRACT

The number of worldwide installed groundwater heat pump (GWHP) systems is approaching one million units. This increase in GWHP systems creates an increasing competition for groundwater use. Thus, we have simulated the long-term thermal impacts of such open-loop geothermal systems with numerical heat transport models, by studying the role of flow and heat transport parameters. The focus is set on transient conditions evolving over decades of seasonally imbalanced heat injections in aquifers with differing ambient flow regimes. The results demonstrate the existence of plume length peaking in moderate groundwater flow velocities (0.5–1.0 m $d^{-1}$). The longitudinal and transverse dispersivity coefficients have a strong influence on the plume extension and on transient development. Reducing the injected temperature difference allows the control of the maximum temperature reached in the plume but implies a considerable hydraulic influence. Comparisons with numerical simulations, using an average of the thermal load, shows that the flow velocity and dispersity coefficients strongly condition the relevance of such simplified approaches. In addition, if satisfactory results are obtained for seasonal or long-term estimations, those for intermediate lengths of time are insufficient. This study contributes to improving the overall understanding of key elements involved in the thermal impact and the development of GWHP systems.

## 1. Introduction

Groundwater heat pumps (GWHP, Fig. 1a) represent a common technology in the field of low-enthalpy geothermal energy utilization. They rely on the presence of groundwater at shallow depths, which is pumped from one or more wells to extract energy for space heating, air conditioning, industrial heat supply, as well as other applications (Rafferty, 2001). The used cooled or warmed water is reinjected into a separate aquifer and ideally, does not interact with the production well. Often, groundwater is also utilized for cooling purposes and therefore water warmer than the originally sourced water is reinjected into the ground. According to Hähnlein et al. (2013) these systems may be further distinguished based on the mode of use. A special category are those applications with the purpose of temporal heat storage such as aquifer thermal storage (ATES) systems (Fleuchaus et al., 2018; Bloemendal and Olsthoorn, 2018; Bloemendal and Hartog, 2018). In the present study however, we focus on GWHP systems that do not consider heat storage. This is mostly the case when groundwater flow is significant and local heat storage is not feasible.

Utilization of groundwater as a heat carrier characterises GWHP systems as open-loop. However, most heat pump-based geothermal systems, are closed-loop systems with vertical borehole heat exchangers (Transparency-Market-Research, 2018; Bayer et al., 2012) (Fig. 1b). In urban environments with productive aquifers, the open-loop GWHPs are growing in numbers. Around every seventh geothermal heat pump is estimated to be an open-loop system (Transparency-Market-Research, 2018). In combination with reported global installed capacity of all geothermal heat pumps in 2015 (Lund and Boyd, 2016), and assuming continued marked growth rates of 10%, the equivalent number of currently installed 12 kW GWHP units has reached more than 800,000 worldwide. As these installations are concentrated primarily in the major cities of countries including USA, China, Sweden, Switzerland, Germany and France, the management of the concurrent use of shallow groundwater resources for various energy supply applications becomes increasingly essential (Hähnlein et al., 2013; Ferguson, 2009; Rivera et al., 2016).

* Corresponding author.
*E-mail address:* guillaume.attard@cerema.fr (G. Attard).

https://doi.org/10.1016/j.geothermics.2019.101721
Received 3 February 2019; Received in revised form 13 August 2019; Accepted 26 August 2019

**Nomenclature**

*Symbol*

| | |
|---|---|
| $C$ | Volumetric heat capacity [J $m^{-3} K^{-1}$] |
| $K$ | Hydraulic conductivity [m $s^{-1}$] |
| $n$ | Porosity [-] |
| $q_h$ | Injected heat power per unit length [W $m^{-1}$] |
| $\bar{q}_h$ | Average value of $q_h$ [W $m^{-1}$] |
| $q_{inj}$ | Injection rate per unit length [$m^3$ $s^{-1}$ $m^{-1}$] |
| $T$ | Calculated front temperature [K] |
| $T_{inj}$ | Temperature of injected water [K] |
| $T_u$ | Undisturbed temperature of aquifer [K] |
| $T_{max}$ | Maximal temperature [K] |
| $\Delta T_{inj}$ | Temperature difference between $T_{inj}$ and $T_u$ [K] |
| $\Delta T$ | Temperature difference between $T$ and $T_u$ [K] |
| $\Delta \overline{T}_{inj}$ | Average value of $\Delta T_{inj}$ [K] |
| $q$ | Specific discharge [m $s^{-1}$] |
| $v_a$ | Groundwater flow velocity ($q$ / $n$) [m $s^{-1}$] |
| $x$ | x-coordinate [m] |
| $y$ | y-coordinate [m] |
| $z$ | z-coordinate [m] |
| $\alpha$ | Dispersivity [m] |
| $\lambda$ | Thermal conductivity [W $m^{-1}$ $K^{-1}$] |

*Subscripts*

| | |
|---|---|
| $s$ | Soil |
| $S$ | Seasonal |
| $l$ | Longitudinal |
| $t$ | Transverse |
| $w$ | Water |
| $Y$ | Yearly |

Regulating multiple adjacent systems, each with slowly evolving thermal effects on the subsurface, is a challenging task. The elementary tools for predicting and managing GWHPs are models that simulate the physical processes in the ground. In recent years, European cities in particular have refined their management strategies of thermal groundwater use through the application of numerical groundwater flow and transport models. Prominent examples of their use are in London (Fry, 2009; Arthur et al., 2010), Zürich, Basel in Switzerland (Epting et al., 2017a; Mueller et al., 2018), Zaragoza in Spain (Epting et al., 2017b; Maya et al., 2018), and Turin in Italy (Sciacovelli et al., 2014; Bucci et al., 2017; Russo et al., 2014) among others. Moreover, Yu et al. (2016) and Liang et al. (2011) showed their results for the Beijing plain and Zhou and Zhou (2009) for Chengdu, China. Rodríguez et al. (2018) inspected GWHP systems for district heating in Puente Alto, Chile. For decades, numerical codes have been used for examination of GWHP thermal impacts in US American cities (e.g. Warner and Algan, 1984). However, often data and technical capacity are inadequate for a detailed simulation. Therefore, models are often calibrated with a limited amount of data and are based on previous experience with similar systems already in use. In such cases, simplification of numerical and analytical models were proposed for a more straightforward analysis of potential thermal breakthrough between well doublets consisting of extraction and injection wells (Lippmann and Tsang, 1980; Gringarten and Sauty, 1975; Casasso and Sethi, 2015; Piga et al., 2017; Milnes and Perrochet, 2013; Banks, 2009; Gandy et al., 2010).

From the perspective of regulators, special attention needs to be given to the potential interaction between neighbouring installations, water protection areas (Haehnlein et al., 2010; Park et al., 2017; Pophillat et al., 2018) as well as groundwater ecosystems (Brielmann et al., 2011). Some related studies have presented sensitivity and scenario analysis of crucial factors for thermal plume development through the employment of analytical and numerical models. For example, Lo Russo et al. (2012) used numerical simulations to carry out a sensitivity analysis by varying hydrogeological and thermal parameters gradually from -20% to +20%, with respect to their real values at a GWHP site. They compared the results from the various scenarios after one year of constant injection. Their results showed that the parameters which have the most significant influence are those related to the advective component of the ground heat flow. However, Piga et al. (2017) employed numerical sensitivity analyses for a more extensive range of parameter values by considering variable injections and longer simulation times of fifty years. They demonstrated that among the hydraulic and thermal parameters, especially the Darcy velocity, thermal conductivity and dispersity, have a significant influence on the plume extension. For a case study, Lo Lo Russo et al. (2014) investigated the role of the temporal discretization of the heat injection for the numerical estimation of the thermal impact. They highlighted the need to consider a temporal resolution that represents a temporal variation of over a year (i.e. hourly to average monthly equivalent) of the injection rate to satisfactorily estimate thermal plume evolution in the aquifer. Piga et al. (2017) also evaluated the ability of numerical models to estimate the thermal impact between well doublets. They concluded that yearly average values can only be used to estimate the plumes in the case of heating or cooling-dominated loads. For more balanced thermal loads, using the yearly averaged load heavily overestimates the plume length and underestimates its width.

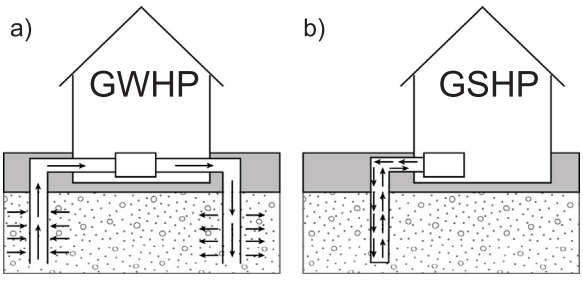


**Fig. 1.** Scheme of open and closed shallow geothermal systems: a) ground water heat pump (GWHP) system and b) ground source heat pump (GSHP).

The findings from previous studies highlight the strong influence of dispersivity. However, the few studies that focus on the long-term thermal impact consider a fixed ratio between longitudinal and transverse dispersivity coefficients. Therefore, the separate influence on the plume evolution is hardly understandable. The influence of parameters that define the heat injection is also rarely studied. Furthermore, the plume extension assessment is mostly based on the use of a fixed temperature difference threshold, for instance, 1 K, along with the potential threshold effect that must be considered.

The present work uses a sensitivity analysis, based on two-dimensional (2D) transient numerical simulations. It aims to deepen the understanding of the influence of the groundwater velocity, the longitudinal and transverse dispersivity coefficients and the parameters used to define the energy load on the long-term thermal impact due to a variable injection. We propose an approach based on the maximal plume extension reached during a cycle of injection, and the influence of the threshold chosen to define the plume boundary is discussed. Also, we specify the range of applicability of simplified averaging of the thermal load depending on the studied parameters. This simplified averaging method contributes to the overarching objective of this study to support authorities in the regulation of GWHP systems in crowded areas, with the help of suitable simplified models.

## 2. Materials and methods

The methodology applied in this work is based on simulation of transient plumes evolving from injection wells. By systematic variation of parameter settings in different theoretical scenarios, the dominant factors for the thermal impact of seasonally operating GWHP systems are revealed. In the following passage the model scenarios are introduced, and the evaluation procedure to compare different model predictions is presented. Additionally, the specifications of the numerical models are described.

### 2.1. Studied scenarios

A porous, homogeneous and confined aquifer with adiabatic upper and lower boundaries is inspected. This aquifer has a porosity of $n = 30\%$, and hydraulic conductivity of $K = 6.94 \times 10^{-4}$ m s$^{-1}$, simulating the typical characteristics of a coarse, sand aquifer (Bayer et al., 2011). The thermal properties are considered homogeneous with a bulk thermal conductivity of the water-saturated aquifer material of $\lambda_m = 2.24$ W m$^{-1}$ K$^{-1}$ (water: 0.578 W m$^{-1}$ K$^{-1}$, solid: 4.0 W m$^{-1}$ K$^{-1}$) and a composite heat capacity of 2.888 MJ m$^{-3}$ K$^{-1}$ (water: 4.185 MJ m$^{-3}$ K$^{-1}$, solid: 2.332 MJ m$^{-3}$ K$^{-1}$) (Woodside and Messmer, 1961). The undisturbed temperature is $T_u = 12$ °C (285.15 K). In different scenarios, further settings are varied based on a reference case with an undisturbed uniform hydraulic gradient of 0.5% which is considered a moderate value for an urban aquifer (Attard et al., 2016a). The resulting groundwater flow velocity (or seepage velocity) is $v_a = 1$ m d$^{-1}$ (which corresponds to a specific discharge of $q = v_a \cdot n = 0.33$ m d$^{-1}$). The default longitudinal and transverse dispersivity of this reference case are set $\alpha_l = 5$ m and $\alpha_t = 0.5$ m, respectively (Stauffer et al., 2013).

In our theoretical study, the implemented GWHP system is only used for cooling during the summer season and is operated for 20 years. The thermal impact from a similar system which was used for heating would be equivalent, but with a cold plume instead of the heat plume simulated here. The assigned time-dependent function for injection is oriented at a realistic air-conditioning demand for a tertiary building located in the area of Lyon (France). In line with the results by Lo Lo Russo et al. (2014) on appropriate temporal discretization, the injection is described by using a modulation function with monthly increments (Fig. 2). Given that the analysis is based on a 2D approach, the various parameters describing the injected heat flux are given per unit length of the injection well. The injected heat flux by unit length of the well $q_h$ considered in the reference scenario is therefore constant over a month, and the value corresponds to the monthly mean of the real injected flux (Fig. 2a). The corresponding water injection is characterized in the reference scenario by a constant temperature difference of $\Delta T_{inj} = 10$ K between groundwater and injected water, and a variable injection rate per unit length of the well, $q_{inj}$. During the injection period, $q_{inj}$ values vary accordingly between 0.01 and 0.12 l s$^{-1}$ m$^{-1}$. Per unit thickness of the aquifer, the annual total volume of water injected is 8172 m$^3$ and the annual total energy content is 3.42 10$^{11}$ J.

Based on the reference case, three distinct influences are configured for the sensitivity analysis resulting in 20 different scenarios (Table 1).

(i) Influence of the groundwater flow velocity: Six scenarios are introduced to evaluate the influence of the ambient groundwater flow velocity. They are implemented by varying the flow velocity of the reference case ($v_a = 1$ m d$^{-1}$) by the factors 0.1, 0.2, 0.5, 2, 5 and 10. The corresponding scenarios are therefore defined by a flow velocity varying between $v_a = 0.1$ m d$^{-1}$ and $v_a = 10$ m d$^{-1}$. These velocities are obtained by keeping the hydraulic gradient at 0.5% and varying the hydraulic conductivity of the aquifer from $6.94 \times 10^{-5}$ m s$^{-1}$ to $6.94 \times 10^{-3}$ m s$^{-1}$. These values correspond to materials varying from very fine sand to coarse gravel (Spitz and Moreno, 1996). Note that groundwater flow velocity varies strongly among different field sites depending on various hydrogeological conditions. Even if two orders of magnitudes are studied for $v_a$, this range does not cover the full scope of observed velocities in practice.

(ii) Influence of the dispersivity coefficients: By revisiting field data reported in the literature, Zech et al. (2015) showed that the longitudinal dispersivity, $\alpha_l$, and in particular its asymptotic value for an extended observation distance, depends strongly on the structural properties of the aquifer. Based on their analysed data sample, this asymptotic value remained lower than 10 m. Furthermore, the survey by Gelhar et al. (1992) demonstrated that the ratio $\alpha_l/\alpha_t$ varies for each case between 1 and 100. Because of these observations, ten scenarios are defined to evaluate the influence of longitudinal and transverse dispersivity. Six of these scenarios investigate the specific role of the transverse dispersivity. The value of $\alpha_l$ is kept at 5 m as in the reference case, and $\alpha_t$ is varied by the factors 0.1, 0.2, 0.5, 2, 5 and 10 (the ratio $\alpha_l/\alpha_t$ thus varies between 1 and 100). Four scenarios inspect the role of the longitudinal dispersivity, $\alpha_l$. According to Zech et al. (2015), its value is kept below 10 m. The transverse dispersivity $\alpha_t$ is set fixed at 0.5 m as in the reference case, and the $\alpha_l$ is varied by the factors 0.1, 0.2, 0.5 and 2, i.e. the anisotropy ratio $\alpha_l/\alpha_t$ thus varies between 1 and 20.

(iii) Influence of parameters describing the heat injection: The injected heat flux per unit length of the injection well is defined by $q_h = q_{inj} C_w \Delta T_{inj}$, where $C_w$ is the heat capacity of water. The variable heat flux (i.e., heat supply by the GWHP) given in Fig. 2a can thus be implemented by varying $q_{inj}$ or $\Delta T_{inj}$. Four scenarios are defined to scrutinize the influence of $q_{inj}$ and $\Delta T_{inj}$ maintaining the similar heat budget. Two scenarios ($\Delta T$-5 and $\Delta T$-2.5) focus on the formulation of a fixed $\Delta T_{inj}$ (5 K and 2.5 K). Accordingly, during the injection period, $q_{inj}$ varies between 0.03 and 0.24 l s$^{-1}$ m$^{-1}$ and 0.06 and 0.48 l s$^{-1}$ m$^{-1}$, respectively. Two further scenarios ($q$-0.12 and $q$-0.24) evaluate the influence of a fixed value of $q_{inj}$ (0.12 l s$^{-1}$ m$^{-1}$). The corresponding values of $\Delta T_{inj}$ vary between 1.2 K and 9.8 K (with a mean value of 5 K), and between 0.6 K and 4.9 K (with a mean value of 2.5 K).

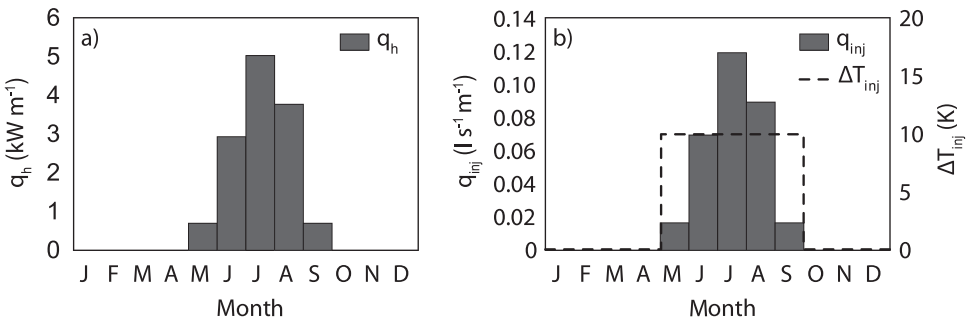


**Fig. 2.** (a) Injected heat flux $q_h$ of reference scenario; (b) corresponding injection rate $q_{inj}$ and temperature difference $\Delta T_{inj}$.

**Table 1**
Definitions and parameter specifications of studied scenarios. Bold values denote those who are varied with respect to the settings of the reference case. Additionally, those physical parameter values are listed, which are kept constant in all scenarios.

| Scenarios | | Parameter values and ranges | | | | |
|---|---|---|---|---|---|---|
| Description | Abbreviation | $q_{inj}$ (l s$^{-1}$ m$^{-1}$) | $\Delta T_{inj}$ (K) | $K$ (m s$^{-1}$) | $\alpha_l$ (m) | $\alpha_t$ (m) |
| *Reference* | Ref. | [0.010.12] | 10 | $6.94 \times 10^{-4}$ | 5 | 0.5 |
| *Influence of the groundwater flow velocity* | | | | | | |
| Reference value × 0.1 | *v*-0.1 | [0.010.12] | 10 | **$6.94 \times 10^{-5}$** | 5 | 0.5 |
| Reference value × 0.2 | *v*-0.2 | [0.010.12] | 10 | **$1.39 \times 10^{-4}$** | 5 | 0.5 |
| Reference value × 0.5 | *v*-0.5 | [0.010.12] | 10 | **$3.47 \times 10^{-4}$** | 5 | 0.5 |
| Reference value × 2 | *v*-2 | [0.010.12] | 10 | **$1.39 \times 10^{-3}$** | 5 | 0.5 |
| Reference value × 5 | *v*-5 | [0.010.12] | 10 | **$3.47 \times 10^{-3}$** | 5 | 0.5 |
| Reference value × 10 | *v*-10 | [0.010.12] | 10 | **$6.94 \times 10^{-3}$** | 5 | 0.5 |
| *Influence of the dispersivity coefficients* | | | | | | |
| Transverse dispersivity | | | | | | |
| Reference value × 0.1 | $\alpha_t$ -0.05 | [0.010.12] | 10 | $6.94 \times 10^{-4}$ | **5** | **0.05** |
| Reference value × 0.2 | $\alpha_t$ -0.1 | [0.010.12] | 10 | $6.94 \times 10^{-4}$ | **5** | **0.1** |
| Reference value × 0.5 | $\alpha_t$ -0.25 | [0.010.12] | 10 | $6.94 \times 10^{-4}$ | **5** | **0.25** |
| Reference value × 2 | $\alpha_t$ -1 | [0.010.12] | 10 | $6.94 \times 10^{-4}$ | **5** | **1** |
| Reference value × 5 | $\alpha_t$ -2.5 | [0.010.12] | 10 | $6.94 \times 10^{-4}$ | **5** | **2.5** |
| Reference value × 10 | $\alpha_t$ -5 | [0.010.12] | 10 | $6.94 \times 10^{-4}$ | **5** | **5** |
| Longitudinal dispersivity | | | | | | |
| Reference value × 0.1 | $\alpha_l$ -0.5 | [0.010.12] | 10 | $6.94 \times 10^{-4}$ | **0.5** | **0.5** |
| Reference value × 0.2 | $\alpha_l$ -1 | [0.010.12] | 10 | $6.94 \times 10^{-4}$ | **1** | **0.5** |
| Reference value × 0.5 | $\alpha_l$ -2.5 | [0.010.12] | 10 | $6.94 \times 10^{-4}$ | **2.5** | **0.5** |
| Reference value × 2 | $\alpha_l$ -10 | [0.010.12] | 10 | $6.94 \times 10^{-4}$ | **10** | **0.5** |
| *Influence of parameters describing the heat injection* | | | | | | |
| Fixed temperature value | | | | | | |
| Reference value × 0.5 | $\Delta T$-5 | **[0.030.24]** | **5** | $6.94 \times 10^{-4}$ | 5 | 0.5 |
| Reference value × 0.25 | $\Delta T$-2.5 | **[0.060.48]** | **2.5** | $6.94 \times 10^{-4}$ | 5 | 0.5 |
| Fixed injection rate | | | | | | |
| $\Delta \bar{T}$ = 5 K | *q*-0.12 | **0.12** | **[1.29.8]** | $6.94 \times 10^{-4}$ | 5 | 0.5 |
| $\Delta \bar{T}$ = 2.5 K | *q*-0.24 | **0.24** | **[0.64.9]** | $6.94 \times 10^{-4}$ | 5 | 0.5 |

**Fixed parameters**

| $i$ (-) | $n$ (-) | $T_u$ (K) | $\lambda_w$ (W m$^{-1}$ K$^{-1}$) | $\lambda_s$ (W m$^{-1}$ K$^{-1}$) | $C_w$ (J m$^{-3}$ K$^{-1}$) | $C_s$ (J m$^{-3}$ K$^{-1}$) |
|---|---|---|---|---|---|---|
| 0.005 | 0.3 | 285.15 | 0.578 | 4 | $4.185 \times 10^6$ | $2.332 \times 10^6$ |

### 2.2. Numerical simulation

Groundwater flow and heat transport are simulated using the commercial code FEFLOW (Diersch, 2014). This software is based on the finite element method and was applied for heat transport in related studies (Epting et al., 2017a; Lo Russo et al., 2014; Attard et al., 2016b; Wagner et al., 2012; Hecht-Méndez et al., 2010; Zhu et al., 2015; Dehkordi and Schincariol, 2014). The 2D numerical model domain used for all scenarios is illustrated in Fig. 3. The domain covers a rectangle of 3000 m by 300 m. Only the injection well is simulated assuming that the production well is located far away from it and that there is no hydraulic interference among them both. The injection well is located at 150 m from the east and north boundaries. A horizontal mesh is applied using a triangular algorithm. The size of the elements ranges from several centimetres near the injection well to about three meters at the domain boundaries.

Fig. 3 shows the boundary conditions (BCs) applied. Concerning the flow problem, Dirichlet BCs (fixed hydraulic head) are assigned to the west and east boundaries, resulting in a forced flow from west to east (Fig. 3). The water injection is simulated by assigning a variable nodal source BC to the well node. Concerning the heat transport problem, Dirichlet BCs (fixed temperature) are set at the east boundary to fix the temperature of the fluid entering through these boundaries. The hot water injection is simulated by implementing a variable heat nodal source BC to the well node and using the divergent form of the heat transport equation (Diersch, 2007). As we focus on a 2D approach, heat conduction into confining layers of the aquifer is not considered. Consequently, all the results are representative for GWHP systems with a sufficiently long well screen.

For each scenario, 20 annual cycles of transient injection are simulated. An annual cycle starts at the beginning of the injection phase (May 1$^{st}$) and lasts 365 days. The hydrogeological and thermal parameters used for the calculations are listed in Table 1.

In order to compare results with a simplifying seasonal average of the energy loads, the models described above are also used with continuous fixed heat injection. The yearly average $\bar{q}_{h\,Y}$ of the thermal load is used with both a one-year and twenty-year simulation time. We also assess the ability to estimate seasonal impact (longer than five months) by using the seasonal average of the thermal load $\bar{q}_{h\,S}$.

### 2.3. Indicators

In the reference case the injection, and thus the shape of the thermal plume, varies throughout an annual cycle. However, after a sufficiently long time at a given location, the plume evolution during a cycle follows the same pattern each year, i.e. the annual trend of the thermal impact is identical. The time it takes to reach this dynamic stability is hereafter called “stabilization time” (St). This is defined as the minimal number of years after which $T$ becomes a periodic (annual) function, meaning that for all points of the studied area and for all $t$>St, we get $T(x, y, t) = T(x, y, t + 1\,\text{year})$.

In our analysis, we focus on the area where the thermal impact

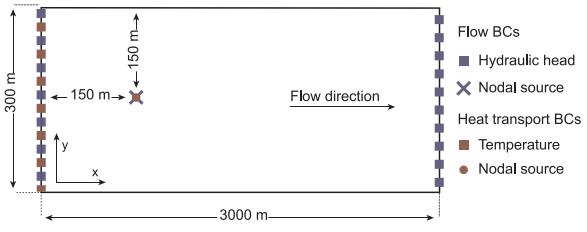


**Fig. 3.** Numerical model geometry, injection well position (nodal source) and boundary conditions (BCs).

exceeds 1 K (1 K-plume), which is commonly used to describe the thermal impact or the so-called thermally affected zone (TAZ) caused by shallow geothermal systems (Piga et al., 2017; Lo Russo et al., 2012, 2014; Molina-Giraldo et al., 2011a, b; Alcaraz et al., 2016). Aside from this, two other thresholds (0.5 K and 2 K) are used to discuss the role of this threshold on the results. For time-dependent management and especially for regulations, maximal effects are of special interest (Hähnlein et al., 2013). The maximal temperature field is thus determined by computing the maximum temperature reached at each point of the domain since the beginning of the simulation:

$$T_{max}(x, y, t_f) = \max_{t\varepsilon\,[0;t_f]} T(x, y, t) \quad (1)$$

Based on this field, the 1 K-max-plume (0.5 K-max-plume and 2 K-max-plume) is defined as the area where the thermal impact exceeds 1 K (0.5 K and 2 K, respectively) at least once since the beginning of the simulation. It expands each new annual cycle and stabilizes when dynamic stability is reached.

Subsequently, we focus on the maximum plume at the end of the simulation ($t_f$), which characterizes the maximal impact reached over the total period of 20 years. For illustration, Figure 4 shows the stabilized shape of 1 K-plumes during the 20$^{th}$ annual cycle and the corresponding 1 K-max-plume.

The plumes extension is analysed based on focusing on the length and maximal width of the plume downgradient from the injection well. Comparisons between scenarios are made by calculating the relative difference between the maximum plume length, width and stabilization time values according to:

$$RD_X = 100 \bullet \frac{X - X_{REF}}{X_{REF}} \% \quad (2)$$

where $X$ denotes the considered parameter (length, width or stabilization time) value and $X_{REF}$ its reference value (i.e. of the reference scenario).

## 3. Results

### 3.1. Simulation of the reference scenario

The final plume of the reference scenario is visualized in Fig. 4b. Ambient groundwater flow moves the thermal plume in the downstream direction. Anisotropic dispersion deforms the plumes and expands them in the longitudinal direction, while together mechanical dispersion and diffusion control continuous spreading. This results in a gradual decrease of the maximum temperature in the downgradient of the well. The 1 K-max-plume length and width are 623 m and 46 m respectively, and it takes six annual cycles to reach the dynamic stability.

However, the thermal effect of the GWHP reaches much further than the 1 K-plume boundary. A crucial determinant for the plume extension is the chosen temperature threshold. To illustrate the role of the threshold, an animation is added in the supplementary material (SI_ref.avi). It illustrates the transient evolution of the 2 K-, 1 K- and 0.5 K-plumes during eight years of injection for reference conditions.

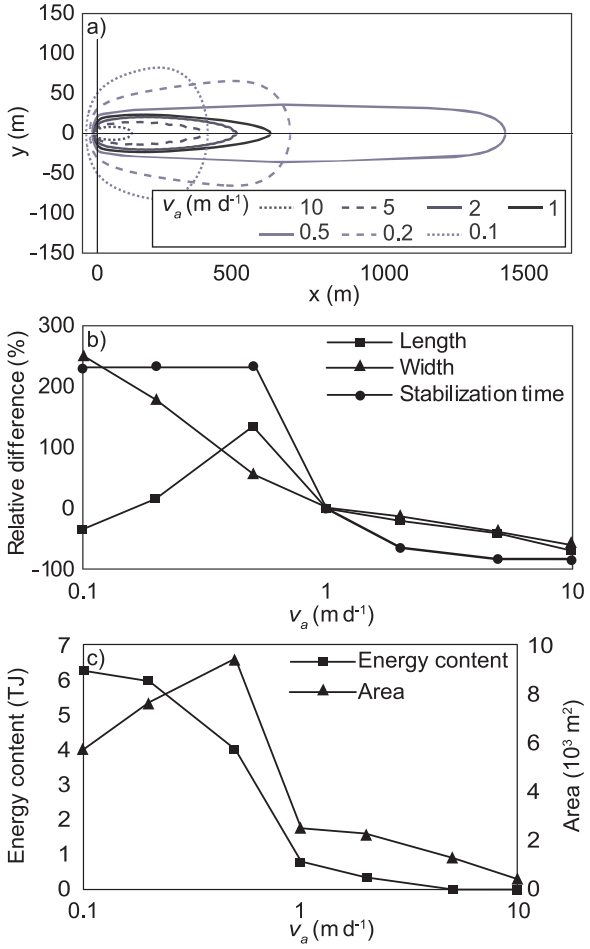


**Fig. 5.** Influence of the groundwater flow velocity: a) 1 K-max-plumes after 20 years; b) relative difference with the reference scenario depending on the flow velocity (x-axis is log scale); c) 1 K-max-plume energy content and area after 20 years depending on the flow velocity (x-axis is log scale).

### 3.2. Influence of groundwater flow velocity

When the groundwater flow velocity is low ($v_a$ = 0.1 m d$^{-1}$), the injection induces a higher local hydraulic gradient around the injection well than for the reference case. It yields a wide 1 K-max-plume

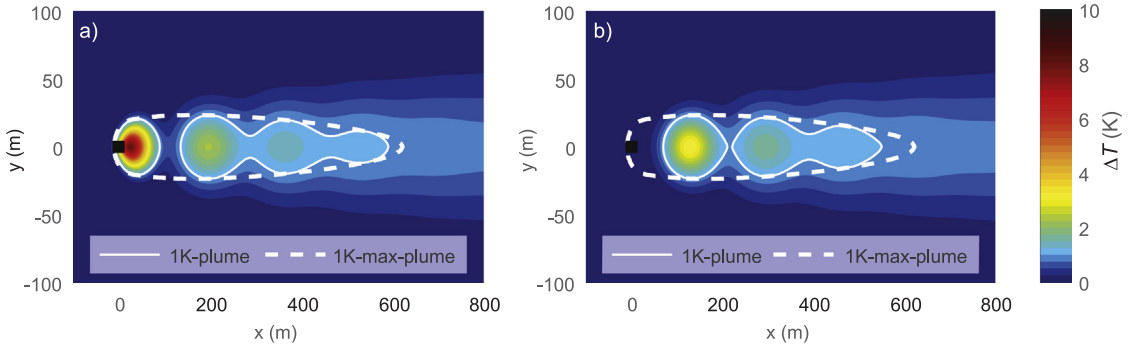


**Fig. 4.** The 20$^{th}$ annual cycle of the reference scenario: 1 K-max-plume and 1 K-plume for a) day 153 (end of the injection phase), and b) day 365 (end of the phase without injection).

characterized by a much higher maximum width (> 250%) and a slightly smaller length. In fact, for flow velocities lower than 0.5 m $d^{-1}$, the dynamic stability is not reached after 20 cycles. Furthermore, the 1 K-max-plumes in Fig. 5 delineate the state of this simulation period, but not steady state conditions.

When increasing the flow velocity in the further scenarios, the local hydraulic effect of the injection well reduces and the hydraulic regime in the aquifer is increasingly dominated by the ambient flow regime. Additionally, higher flow velocities induce more mechanical dispersion, both in the longitudinal and in the transversal direction. The plume gets gradually thinner when the flow velocity increases. Also, the 1 K-max-plume length grows and reaches a peak value for a flow velocity between $v_a = 0.5$ m $d^{-1}$ and $v_a = 1$ m $d^{-1}$. For a flow velocity of 0.5 m $d^{-1}$, the maximum plume length reaches 1463 m. It drops to 623 m for $v_a = 1$ m $d^{-1}$ and for higher velocities the length of the 1 K-max-plume and the stabilization time gradually decrease. In comparison, the relative shrinking of the plume width is less pronounced. For a very high groundwater flow velocity of 10 m $d^{-1}$, the plume is very small. The high dispersion associated with this velocity results in a large spreading of the injected heat and the maximum temperature quickly falls below 1 K following the completion of a heat injection phase.

Computing the Peclet number for each of these scenarios shows that they are always characterized by an advection dominated heat transport. Results show the existence of a limit velocity value (between 0.5 and 1 m $d^{-1}$) beyond which a sharp decline of the 1 K-max-plume length (Fig. 5b), area and energy content (Fig. 5c) are observed. As illustrated in Fig. 5a, the plume area declines at higher flow velocity as a consequence of growing longitudinal spreading. At lower flow velocity, the effect of dispersive spreading diminishes, yielding a maximum of plume length and surface at $v_a = 0.5$ m $d^{-1}$. As smaller flow velocity and thus advection attenuates downgradient propagation of the plume, plume length and area decrease again. Under such conditions, conduction has a significant effect on the heat transport but obviously is less influential than advection and dispersion. In fact, the energy content within the 1 K-max-plume rises when lowering the flow velocity. This reflects that the plume may be deformed by advection, but its energy content is mostly linked to the dispersive spreading of the plume. Increase of ambient flow velocity thus yields a variable plume size depending mainly on advection and dispersion, whereas the energy content is governed by dispersion. Small plumes in case of small velocity thus have relatively high temperatures. The associated enhanced lateral conduction, however, does not substantially influence the energy content of the plume. The reversal points in the curves shown in Figs. 5b,c depend on the temperature threshold. The higher the threshold, the smaller the velocity value corresponding to the reversal point (Fig. 6).

### 3.3. Influence of dispersivity coefficients

We keep the reference settings and focus on the effect of the transverse and longitudinal dispersivity coefficients. We thus consider the variation of the dispersion in each direction separately. The influence of dispersivity values on 1 K-max plumes is shown in Fig. 7. Also, two Figures (S2 and S3) were added as supplementary material to understand the individual role played by $\alpha_l$ and $\alpha_t$. They show the 1 K plumes (instead of 1 K-max-plumes) at the end of each month of the 20$^{th}$ annual cycle of injection for the scenarios related to the longitudinal and transverse dispersivity coefficients.

The influence of the longitudinal dispersivity value on the 1 K-max-plume extension is shown by Fig. 7a and c. In these scenarios, the transverse dispersivity is kept at $\alpha_t = 0.5$ m. Results show that the lowest $\alpha_l$ considered ($\alpha_l = 0.5$ m) causes a long 1 K-max-plume, which is 99% longer than for the reference case and has a higher stabilization time. When $\alpha_l$ increases, the 1 K-max-plume length gradually decreases. For $\alpha_l \geq 2.5$ m, the relative influence of longitudinal dispersivity variation becomes less pronounced (Fig. 7c). It also has a reduced influence on the 1 K-max-plume width and on the stabilization time (Fig. 7c).

The influence of the transverse dispersivity value on the 1 K-max-plume extension is shown by Fig. 7b and d. In these scenarios, the longitudinal dispersivity is kept at $\alpha_l = 5$ m. The lowest $\alpha_t$ yields a thin and long 1 K-max-plume (Fig. 7b), which is 165% longer than for the reference case and has a high stabilization time. When $\alpha_t$ increases, the 1 K-max-plume width also increases and its length greatly decreases (Fig. 7b). The stabilization time also declines. The relative influence of $\alpha_t$ on plume length, width and stabilization time is significantly more pronounced than for $\alpha_l$. For the considered ranges, the 1 K-max-plume lengths are between 177 m and 1655 m for variable $\alpha_t$, and between 598 m and 1242 m when changing $\alpha_l$, indicating a considerable influence of transverse dispersivity.

Complementary information of the influence of the dispersivity values can be obtained by focusing on the fate of the plumes generated by subsequent injection phases (Figure S2). Increasing $\alpha_l$ (or $\alpha_t$) (i.e. increasing the plume spreading in longitudinal (or transverse) direction) conducts to accelerate the decrease of the energy concentration into the plume and consequently, to reduce the distance from which its maximal temperature passes below 1 K (Figure S2). Again, the temperature threshold is elementary for the derived ranges. As can be seen from Fig. 8a, the higher the threshold, the higher the relative influence of $\alpha_l$ is, and by contrast, the lower the relative influence of $\alpha_t$ is.

### 3.4. Characteristics of the heat injection

Fig. 9 depicts the results for changing the heat injection by modifying the temperature difference $\Delta T_{inj}$ and the injection rate, $q_{inj}$. When reducing $\Delta T_{inj}$ we increased $q_{inj}$ to keep the same power of injection. The stronger hydraulic effect of injection generates more radial spreading and thus a greater plume width. Therefore, the lower the value of $\Delta T_{inj}$, the shorter, but the wider the 1 K-max-plume is, especially close to the injection well. For instance, for a fixed $\Delta T_{inj}$ of 2.5 K the 1 K max plume is almost 30% shorter and 50% wider than in the reference scenario.

Using a fixed $q_{inj}$ of 0.12 l $s^{-1}$ $m^{-1}$ implies setting a $\Delta T_{inj}$ that varies between 1.2 K and 9.8 K with a mean value of 5 K. As can be seen from Fig. 9, it yields a 1 K-max-plume that lies between those generated by injection with constant $\Delta T_{inj}$ of 5 K and 10 K. Also, a fixed $q_{inj}$ of 0.24 l $s^{-1}$ $m^{-1}$ implies setting a $\Delta T_{inj}$ that varies between 0.6 K and 4.9 K with a mean value of 2.5 K. It yields a 1 K-max-plume extension between those from plumes generated by injection with constant $\Delta T_{inj}$ of 2.5 K and 5 K. Therefore, when $\Delta T_{inj}$ varies during the injection (between its minimal value $\Delta T_{min}$ and its maximal $\Delta T_{max}$ with an average value $\overline{\Delta T}$), the 1 K-plume extension is between those generated by an identical heat injection with a fixed temperature difference $\Delta T_{inj} = \Delta T_{max}$ and $\Delta T_{inj} = \overline{\Delta T}$.

### 3.5. Seasonal averaging of the injection

Fig. 10 shows the relative difference on the 1 K-max-plume extension obtained by considering the variable thermal load or its seasonal

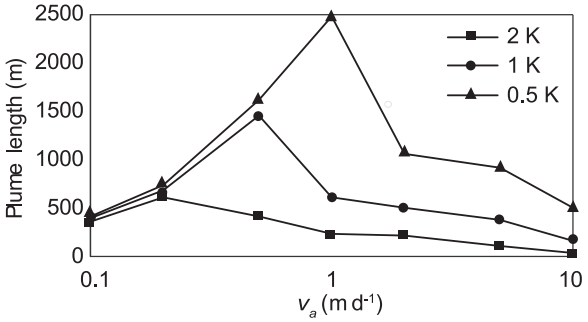


**Fig. 6.** Absolute lengths of the 0.5 K, 1 K and 2 K-max-plumes depending on the groundwater flow velocity (x-axis is log scale).

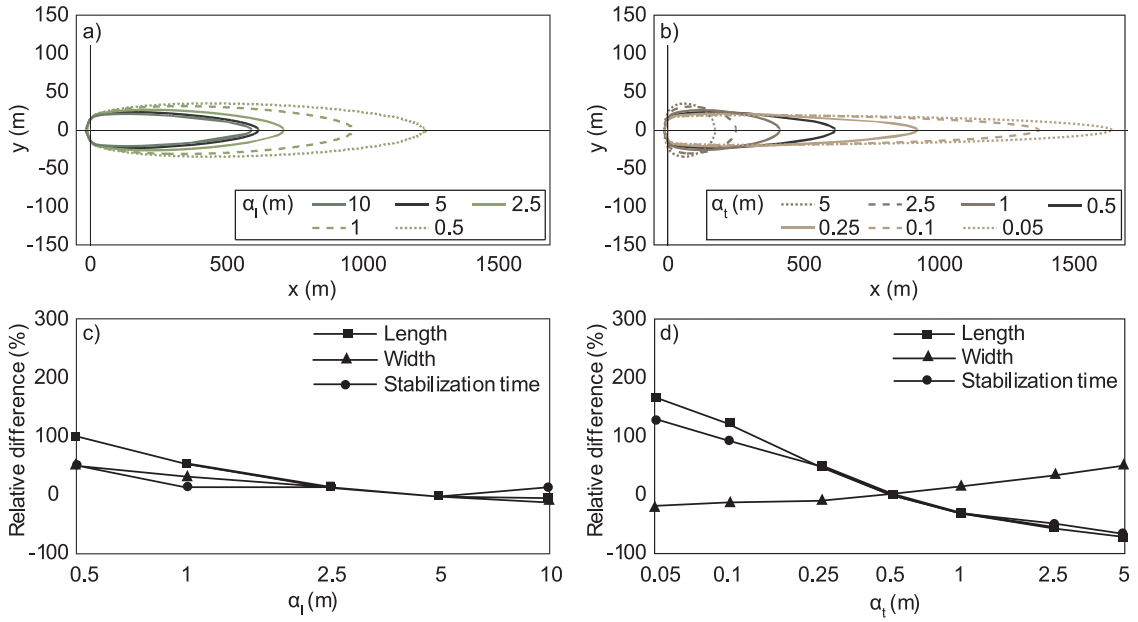


**Fig. 7.** Influence of the dispersity coefficient. 1 K-max-plumes after 20 years for various values of $\alpha_l$ (a) and $\alpha_t$ (b). Relative difference compared to the reference scenario for various values of $\alpha_l$ (c) and $\alpha_t$ (d) (horizontal axis is log scale).

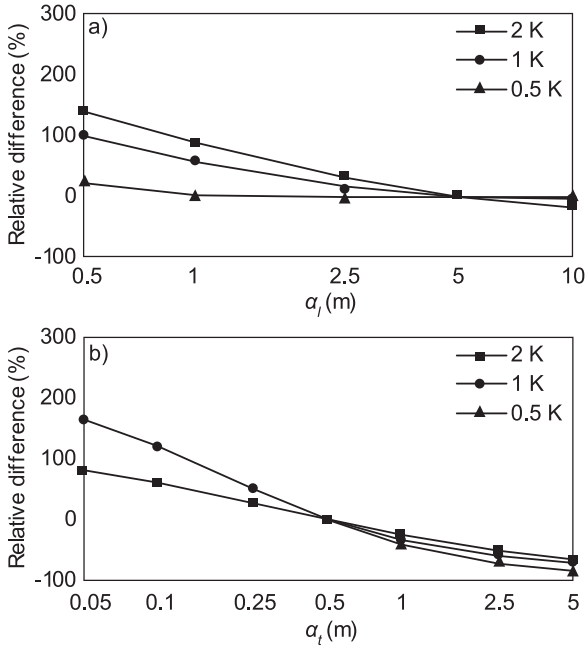


**Fig. 8.** Influence of the threshold choice on the dispersivity coefficients influence evaluated as relative difference with the reference scenario (x-axis is log scale): a) longitudinal dispersivity; b) transverse dispersivity (length values for transverse dispersivity below 0.5 m exceed the domain size).

average. ·The simplified model estimates are evaluated for the various scenarios (except q-0.12 and q-0.24) after five months (using the seasonal average of the load $\bar{q}_{h\,s}$), one year and twenty years (using the yearly average of the load, $\bar{q}_{h\,y}$).

Estimating the seasonal impact (at five months) using a constant load $\bar{q}_{h\,s}$ yields satisfactory results (relative error < 20%), except for cases when the groundwater flow velocity > 2 m $d^{-1}$ (see Fig. 9a). Overall, the plume width is underestimated and its length overestimated. This resulting trend is reinforced by the increase of the flow velocity and reflects the increase of relative importance of the injection peak on the plume development.

As seen in Fig. 10, using the yearly average of the thermal load $\bar{q}_{h\,y}$ to estimate the thermal impact after a year yields less accurate results. The quality of the results increases with the time until the dynamic stability state is reached. However, determining the long-term impact by means of $\bar{q}_{h\,y}$ yields satisfactory results only for a groundwater flow velocity lower than 1 m $d^{-1}$, a longitudinal dispersivity coefficient higher than 5 m, a transverse dispersivity higher lower than 0.5 m and a temperature difference higher than 5 K. Outside this range, the quality of the estimation dramatically decreases.

## 4. Discussion

The influence of the background velocity has been assessed by using an extensive range of groundwater flow velocities representative of realistic hydrogeological conditions. Our results confirm previous findings that show the strong influence of the background velocity on the seasonal plume shape and its long-term evolution (Piga et al., 2017; Russo et al., 2012). We found a similar trend for the maximal plume width. However, in contrast to previous studies, our results show the existence of a peak for the maximal length.

The present study provides the first insight into the individual influence of the longitudinal and transverse dispersivity coefficients on the thermal plume caused by a long-term variable injection of hot water. By varying both longitudinal and transverse coefficients separately within realistic ranges, we demonstrate their strong influence. Nevertheless, the longitudinal dispersivity does not have a substantial influence on the plume width. The influence of a relative increase of the longitudinal dispersivity on the plume length decreases for values over 2.5 m, which is less pronounced for the transverse dispersivity. Overall, the latter has a significantly stronger influence on both plume extension and stabilization time. As shown in previous studies, $\alpha_t$ is the main driver for mixing with pristine groundwater (Zhu et al., 2015). By using a simultaneous variation of both parameters with a constant ratio of 10 between longitudinal and transverse dispersivity, Piga et al. (2017) found that varying the longitudinal dispersivity below 2 m is negligible for the plume extension. We do not observe such a trend for a separate variation of the parameters and thus further studies should be done to deepen the understanding of the influence of the degree of anisotropy in mechanical dispersion.

For all presented scenario groups, results highlight the crucial role

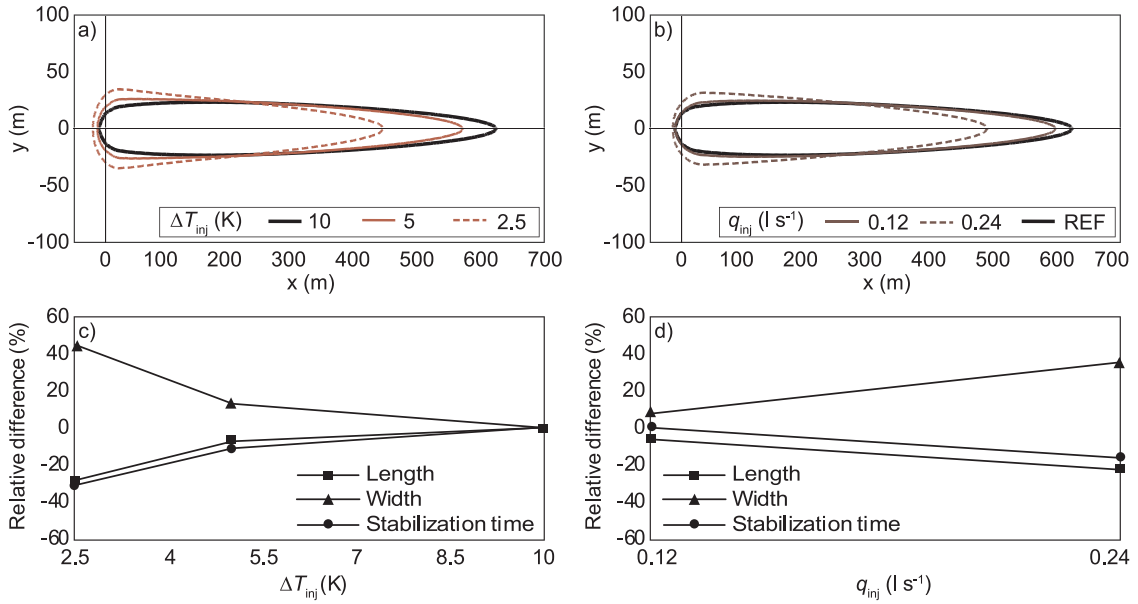


**Fig. 9.** Influence of the characteristics of the heat injection: 1 K-max-plumes after 20 years for scenarios considering a fixed $\Delta T_{inj}$ (a) and a fixed $q_{inj}$ (b); relative difference with the reference scenario for scenarios considering a fixed $\Delta T_{inj}$ (c) and a fixed $q_{inj}$ (d).

of the temperature threshold chosen to qualify and understand the impact of the key parameters. On the one hand, the resulting physical parameters' influence may be different. On the other hand, these parameters influence the plume spread and therefore the distance between the computed plume isotherms. When considering the operational management of a large number of installations, the suitability of referring to arbitrary thresholds should be reconsidered. An example to improve this would be at the least to inspect plume fringes within threshold ranges.

The maximal annual temperature field as proposed in this work, facilitates the understanding of the parameters' role by providing a representation that is easier to interpret than a transient plume. In addition, it avoids underestimations of the plume extension which could occur when considering instantaneous plumes in time and it is therefore suitable for operational purposes. In practice however, it may be of interest to monitor and manage the seasonal or long-term transient plume evolution of GWHP systems in detail.

This work is intended to focus on the specific role of various parameters. Given this objective, it is based on the use of two-dimensional (2D) numerical models. If the influence of vertical heat exchange

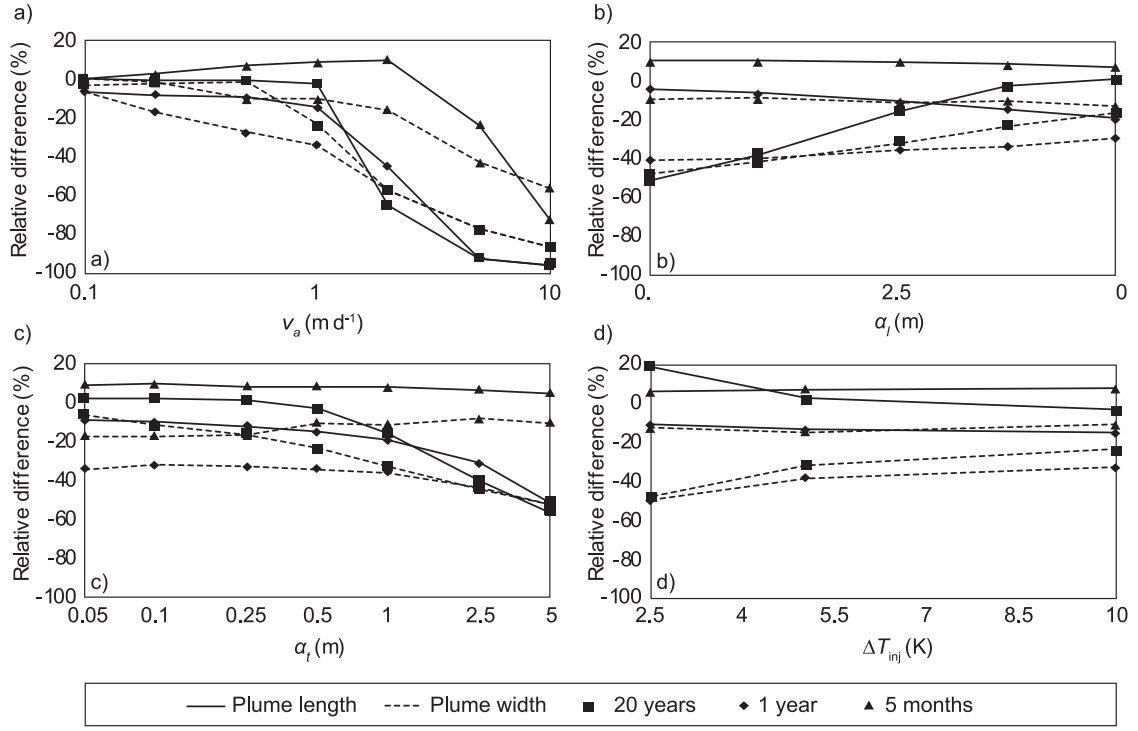


**Fig. 10.** Relative difference on the 1 K-max-plume extension computed using a variable thermal load (reference) and a constant load: a) Influence of the groundwater flow velocity (x-axis is log scale); b) influence of the longitudinal dispersivity; c) influence of the transverse dispersivityd) influence of the injected temperature difference.

cannot be neglected in the assessment of long-term thermal impacts (Piga et al., 2017), they are expected to attenuate the plume extension and the sensitivity of the plume evolution on the parameters studies here. Further analyses should be done with three-dimensional (3D) models to scrutinize vertical heat loss and also to examine the role of further processes such as hydraulic recharge from rainfall.

## 5. Conclusions

The number of groundwater heat pumps (GWHP) systems has sharply increased during this last decade potentially leading to cumulative thermal impacts in several urban settings. However, these systems generate thermal impacts that strongly depend on their size, as well as on the present hydrogeological conditions. As these thermal impacts are likely to affect the efficiency of neighbouring installations, a good understanding of the role of various site-specific parameters on the thermal plume evolution is required to set up adapted management strategies. Our results deepen the knowledge of the role of the flow velocity, the longitudinal and transverse dispersity and the parameters used to describe the heat injection.

We demonstrate the strong influence of the groundwater flow velocity on both plume extension as well as the time it takes to reach a dynamic stability state. We also highlight the non-monotonous relation between the velocity and the plume length and width, with a peak that occurs for moderate flow velocity (0.5–1.0 m $d^{-1}$). By contrast, the plume width gradually decreases when the velocity increases and the overall lowest extension and stabilization time is obtained for high flow velocities ($>>1$ m $d^{-1}$). The dispersivity influence has been inspected by separately varying the longitudinal and transverse coefficients in a broad, realistic range. The longitudinal dispersivity has no significant influence on the plume width and stabilization time. Its influence on the length is strong for low values, and it decreases remarkably for a values over 2.5 m. In comparison, the transverse dispersivity has a more pronounced influence on the plume length, width and on the stabilization time.

Several scenarios were used to inspect the influence of the parameters defining the variable injection mode of a GWHP system. Our results show that if the maximal temperature difference reached within the plume can be kept under a threshold (by adjusting $\Delta T_{inj}$), the hydraulic impact will be higher. For a threshold below $\Delta T_{inj}$ the plume will be shorter but wider close to the well compared to when obtained with an identical power injection using a higher $\Delta T_{inj}$. Therefore, such a strategy could be used to avoid thermal interference with neighbouring installations in urban areas.

Simplified models considering the seasonal average of the thermal load have been tested in order to specify their range of applicability. The groundwater flow velocity, as well as the dispersity coefficients, strongly condition the relevance of the seasonal averaging. Also, if satisfactory results are obtained for seasonal or long-term estimations, results for mid-lengths of time are weaker. If such models cannot precisely determine the actual shape of the plume, in their scope of applicability they can yield satisfactory estimates of the maximal impact within a short simulation time. This makes such models suitable for supporting GWHP management in the field. However, considering the relative errors obtained, they should only be used for first-tier assessment of the thermal impact. Additionally, the applicability of analytical solutions such as those proposed by Pophillat et al. (2018) should be scrutinized for long-term assessment.

This study highlights the advantages of considering the annual maximal temperature field to represent the thermal plume generated by a variable injection. Our results also demonstrate the considerable influence of the given temperature threshold to delineate the plume boundary. Accordingly, spatial management of GWHP systems should not rely on arbitrary thresholds but should compare the role of different thresholds on the computed isotherms, or ideally should consider the full temperature field that is evolving from GWHP systems.

## Declaration of Competing Interest

The authors declare that there are no conflicts of interest.

## Acknowledgements

This work was supported by the German Research Foundation (project number BA2850/3-1) and by the French Ministry of Ecological and Solidarity Transition. We thank Kristie Ussher and Enzio Schoffer for language corrections. Finally, we also would like to thank the two anonymous reviewers for the constructive and useful comments.

## Appendix A. Supplementary data

Supplementary material related to this article can be found, in the online version, at doi:https://doi.org/10.1016/j.geothermics.2019.101721.

## References

Alcaraz, M., García-Gil, A., Vázquez-Suñé, E., Velasco, V., 2016. Advection and dispersion heat transport mechanisms in the quantification of shallow geothermal resources and associated environmental impacts. Sci. Total Environ. 543, 536–546.
Arthur, S., Streetly, H., Valley, S., Streetly, M., Herbert, A., 2010. Modelling large ground source cooling systems in the Chalk aquifer of central London. Q. J. Eng. Geol. Hydrogeol. 43 (3), 289–306.
Attard, G., Winiarski, T., Rossier, Y., Eisenlohr, L., 2016a. Impact of underground structures on the flow of urban groundwater. Hydrogeol. J. 24 (1), 5–19.
Attard, G., Rossier, Y., Winiarski, T., Eisenlohr, L., 2016b. Deterministic modeling of the impact of underground structures on urban groundwater temperature. Sci. Total Environ. 572, 986–994.
Banks, D., 2009. Thermogeological assessment of open-loop well-doublet schemes: a review and synthesis of analytical approaches. Hydrogeol. J. 17 (5), 1149–1155.
Bayer, P., Huggenberger, P., Renard, P., Comunian, A., 2011. Three-dimensional high resolution fluvio-glacial aquifer analog: part 1: field study. J. Hydrol. 405 (1–2), 1–9.
Bayer, P., Saner, D., Bolay, S., Rybach, L., Blum, P., 2012. Greenhouse gas emission savings of ground source heat pump systems in Europe: a review. Renew. Sustain. Energy Rev. 16 (2), 1256–1267.
Bloemendal, M., Hartog, N., 2018. Analysis of the impact of storage conditions on the thermal recovery efficiency of low-temperature ATES systems. Geothermics 71, 306–319.
Bloemendal, M., Olsthoorn, T., 2018. ATES systems in aquifers with high ambient groundwater flow velocity. Geothermics 75, 81–92.
Brielmann, H., Lueders, T., Schreglmann, K., Ferraro, F., Avramov, M., Hammerl, V., Blum, P., Bayer, P., Griebler, C., 2011. Shallow geothermal energy usage and its potential impacts on groundwater ecosystems. Grundwasser 16 (2), 77–91.
Bucci, A., Barbero, D., Lasagna, M., Forno, M.G., De Luca, D.A., 2017. Shallow groundwater temperature in the Turin area (NW Italy): vertical distribution and anthropogenic effects. Environ. Earth Sci. 76 (5), 221.
Casasso, A., Sethi, R., 2015. Modelling thermal recycling occurring in groundwater heat pumps (GWHPs). Renew. Energy 77, 86–93.
Dehkordi, S.E., Schincariol, R.A., 2014. Effect of thermal-hydrogeological and borehole heat exchanger properties on performance and impact of vertical closed-loop geothermal heat pump systems. Hydrogeol. J. 22 (1), 189–203.
Diersch, H., 2007. About the Difference between the Convective Form and the Divergence Form of the Transport Equation in FEFLOW White Papers Vol. I DHI-WASY GmbH, Berlin, Germany.
Diersch, H.-J.G., 2014. FEFLOW: Finite Element Modeling of Flow, Mass and Heat Transport in Porous and Fractured Media. Springer, Berlin.
Epting, J., Scheidler, S., Affolter, A., Borer, P., Mueller, M.H., Egli, L., García-Gil, A., Huggenberger, P., 2017a. The thermal impact of subsurface building structures on urban groundwater resources–a paradigmatic example. Sci. Total Environ. 596, 87–96.
Epting, J., García-Gil, A., Huggenberger, P., Vázquez-Suñe, E., Mueller, M.H., 2017b. Development of concepts for the management of thermal resources in urban areas–Assessment of transferability from the Basel (Switzerland) and Zaragoza (Spain) case studies. J. Hydrol. 548, 697–715.
Ferguson, G., 2009. Unfinished business in geothermal energy. GroundWater 47 (2) 167-167.
Fleuchaus, P., Godschalk, B., Stober, I., Blum, P., 2018. Worldwide application of aquifer thermal energy storage–a review. Renew. Sustain. Energy Rev. 94, 861–876.
Fry, V., 2009. Lessons from London: regulation of open-loop ground source heat pumps in central London. Q. J. Eng. Geol. Hydrogeol. 42 (3), 325–334.
Gandy, C., Clarke, L., Banks, D., Younger, P., 2010. Predictive modelling of groundwater abstraction and artificial recharge of cooling water. Q. J. Eng. Geol. Hydrogeol. 43 (3), 279–288.
Gelhar, L.W., Welty, C., Rehfeldt, K.R., 1992. A critical review of data on field-scale dispersion in aquifers. Water Resour. Res. 28 (7), 1955–1974.
Gringarten, A., Sauty, J., 1975. A theoretical study of heat extraction from aquifers with uniform regional flow. J. Geophys. Res. 80 (35), 4956–4962.

Haehnlein, S., Bayer, P., Blum, P., 2010. International legal status of the use of shallow geothermal energy. Renew. Sustain. Energy Rev. 14 (9), 2611–2625.
Hähnlein, S., Bayer, P., Ferguson, G., Blum, P., 2013. Sustainability and policy for the thermal use of shallow geothermal energy. Energy Policy 59, 914–925.
Hecht-Méndez, J., Molina-Giraldo, N., Blum, P., Bayer, P., 2010. Evaluating MT3DMS for heat transport simulation of closed geothermal systems. Ground Water 48 (5), 741–756.
Liang, J., Yang, Q., Liu, L., Li, X., 2011. Modeling and performance evaluation of shallow ground water heat pumps in Beijing plain, China. Energy Build. 43 (11), 3131–3138.
Lippmann, M.J., Tsang, C.F., 1980. Ground-water use for cooling: associated aquifer temperature changes. Groundwater 18 (5), 452–458.
Lo Russo, S., Taddia, G., Verda, V., 2012. Development of the thermally affected zone (TAZ) around a groundwater heat pump (GWHP) system: a sensitivity analysis. Geothermics 43, 66–74.
Lo Russo, S., Gnavi, L., Roccia, E., Taddia, G., Verda, V., 2014. Groundwater Heat Pump (GWHP) system modeling and Thermal Affected Zone (TAZ) prediction reliability: influence of temporal variations in flow discharge and injection temperature. Geothermics 51, 103–112.
Lund, J.W., Boyd, T.L., 2016. Direct utilization of geothermal energy 2015 worldwide review. Geothermics 60, 66–93.
Maya, S.M., García-Gil, A., Schneider, E.G., Moreno, M.M., Epting, J., Vázquez-Suñé, E., Marazuela, M., Sánchez-Navarro, J., 2018. An upscaling procedure for the optimal implementation of open-loop geothermal energy systems into hydrogeological models. J. Hydrol.
Milnes, E., Perrochet, P., 2013. Assessing the impact of thermal feedback and recycling in open-loop groundwater heat pump (GWHP) systems: a complementary design tool. Hydrogeol. J. 21 (2), 505–514.
Molina-Giraldo, N., Bayer, P., Blum, P., 2011a. Evaluating the influence of thermal dispersion on temperature plumes from geothermal systems using analytical solutions. Int. J. Therm. Sci. 50 (7), 1223–1231.
Molina-Giraldo, N., Blum, P., Zhu, K., Bayer, P., Fang, Z., 2011b. A moving finite line source model to simulate borehole heat exchangers with groundwater advection. Int. J. Therm. Sci. 50 (12), 2506–2513.
Mueller, M.H., Huggenberger, P., Epting, J., 2018. Combining monitoring and modelling tools as a basis for city-scale concepts for a sustainable thermal management of urban groundwater resources. Sci. Total Environ. 627, 1121–1136.
Park, B.-H., Ha, S.-W., Lee, K.-K., 2017. Minimum Well Separation for Small Groundwater Heat Pump (GWHP) Systems in Korea: Preliminary Analysis Based on Regional Aquifer Properties.
Pophillat, W., Attard, G., Bayer, P., Hecht-Méndez, J., Blum, P., 2018. Analytical solutions for predicting thermal plumes of groundwater heat pump systems. Renew. Energy (accepted).
Piga, B., Casasso, A., Pace, F., Godio, A., Sethi, R., 2017. Thermal impact assessment of groundwater heat pumps (GWHPs): rigorous vs. simplified models. Energies 10 (9), 1385.
Rafferty, K., 2001. Design Aspects of Commercial Open-loop Heat Pump Systems.
Rivera, J., Benz, S., Blum, P., Bayer, P., 2016. Increased temperature in urban ground As source of sustainable energy. Int. J. Energy Prod. Manag. 1 (3), 263–271.
Rodríguez, V., Muñoz, M., Frederick, R., Maturana, B., 2018. District heating by Groundwater Heat Pump in a social integration housing project located in Puente Alto, Central Chile.
Russo, S.L., Taddia, G., Verda, V., 2012. Development of the thermally affected zone (TAZ) around a groundwater heat pump (GWHP) system: a sensitivity analysis. Geothermics 43, 66–74.
Russo, S.L., Gnavi, L., Roccia, E., Taddia, G., Verda, V., 2014. Groundwater Heat Pump (GWHP) system modeling and Thermal Affected Zone (TAZ) prediction reliability: influence of temporal variations in flow discharge and injection temperature. Geothermics 51, 103–112.
Sciacovelli, A., Guelpa, E., Verda, V., 2014. Multi-scale modeling of the environmental impact and energy performance of open-loop groundwater heat pumps in urban areas. Appl. Therm. Eng. 71 (2), 780–789.
Spitz, K., Moreno, J., 1996. A Practical Guide to Groundwater and Solute Transport Modeling. John Wiley, New York.
Stauffer, F., Bayer, P., Blum, P., Giraldo, N., Kinzelbach, W., 2013. Thermal Use of Shallow Groundwater. CRC Press.
Transparency-Market-Research, https://globenewswire.com/news-release/2015/02/02/702002/10118074/en/Global-Geothermal-Heat-Pump-Installed-Capacity-and-Market-Revenue-is-Anticipated-to-reach-119-303-66-MWt-and-USD-130-50-billion-respectively-by-2020-Transparency-Market-Research.html, 2018. (Accessed 02.08. 2018.
Wagner, V., Bayer, P., Kübert, M., Blum, P., 2012. Numerical sensitivity study of thermal response tests. Renew. Energy 41, 245–253.
Warner, D.L., Algan, U., 1984. Thermal impact of residential ground-water heat pumps. Groundwater 22 (1), 6–12.
Woodside, W., Messmer, J., 1961. Thermal conductivity of porous media. I. Unconsolidated sands. J. Appl. Phys. 32 (9), 1688–1699.
Yu, Z., Zhang, Y., Hao, S., Zhang, J., Li, X., Cai, B., Xu, T., 2016. Numerical study based on one-year monitoring data of groundwater-source heat pumps primarily for heating: a case in Tangshan, China. Environ. Earth Sci. 75 (14), 1070.
Zech, A., Attinger, S., Cvetkovic, V., Dagan, G., Dietrich, P., Fiori, A., Rubin, Y., Teutsch, G., 2015. Is unique scaling of aquifer macrodispersivity supported by field data?: Is unique scaling supported by field data? Water Resour. Res. 51 (9), 7662–7679.
Zhou, Y., Zhou, Z., 2009. Simulation of thermal transport in aquifer: a GWHP system in Chengdu, China. J. Hydrodynam. 21 (5), 647–657.
Zhu, K., Bayer, P., Grathwohl, P., Blum, P., 2015. Groundwater temperature evolution in the subsurface urban heat island of Cologne, Germany. Hydrol. Process. 29 (6), 965–978.